Available at www.ComputerScienceWeb.com
POWERED BY SCIENCE DIRECT®

Pattern Recognition Letters 24 (2003) 729–739

Pattern Recognition Letters

www.elsevier.com/locate/patrec

Is early detection of liver and breast cancers from ultrasound scans possible? ☆

G. Georgiou [a,*], F.S. Cohen [b]

[a] European Patent Office, The Hague, The Netherlands
[b] Imaging and Computer Vision Center, Department of Electrical and Computer Engineering, Drexel University, Philadelphia, PA 19104 USA

Abstract

This paper presents an integral approach for the tissue characterization problem. Such an approach includes a model, estimation algorithms and an evaluation method. This work focuses on liver and breast tissue characterization but it may be applicable to other tissue types after proper modifications. Liver and breast tissue is composed of two major kinds of scattering structure, i.e., the liver and breast parenchyma, which is relatively large and thus resolvable using the current ultrasonic transducers, and liver and breast cells which are not resolvable. In this work, we propose a decomposition approach for the RF echo into two components, namely the coherent and diffuse component, which are related to the resolvable and unresolvable scatterers in the liver and breast structure, respectively. Structural differences between the liver and breast, related to the resolvable scatterers properties, led us to develop two different decomposition algorithms. The first algorithm was developed for the liver RF echo and was based on the quasi-periodic structure of the liver lobules. Breast tissue decomposition was based on a more general model for the resolvable scatterers echo, because the breast tissue parenchyma is far from regular. By using the proposed decomposition we were able to estimate structural parameters of the liver and breast such as the average spacing of the liver lobules, the energy of the resolvable and unresolvable scatterers, and the correlation between neighboring unresolvable scatterers in the tissue. Empirical receiver operating characteristics analysis was applied to the parameters estimated from a large database of liver and breast B-scan images, to evaluate their diagnostic power. Single parameters of the liver and breast tissue showed good discriminating power between cancerous and normal liver and breast tissue, and also between malignant and benign breast tissue. The ability to identify small breast lesions (4 mm) is also demonstrated.

Keywords: Tissue characterization; Coherent scatterers; Diffuse scatterers; Wold decomposition; Minimum mean square; Wavelet transform; Empirical receiver operating characteristics curves

1. Introduction

Ultrasonography is an imaging modality that is non-invasive and painless, it is real time, it is of low cost, and it is safe for the patient. Nevertheless, its diagnostic value for breast and liver cancer

☆ This work is supported by the National Cancer Institute and the National Institutes of Health under grant number CA52823.
* Corresponding author.

0167-8655/03/$ - see front matter © 2002 Published by Elsevier Science B.V.
PII: S0167-8655(02)00178-2

detection is limited because of the low resolution of the imaging system with respect to the tissue structures, that results in difficult visual differentiation between normal and pathologic tissue, especially at the early stages of cancer formation (<5 mm). The resolution can be increased by increasing the central frequency of the transducer, but in this case we observe high attenuation resulting in limited penetration depth, which makes the examination of deep organs impossible. Hence, in order to ultrasonographically examine organs such as the liver, we have to compromise with limited resolution.

To improve the usefulness of ultrasound in early diagnosis of cancer a lot of attention has been focused in developing quantitative methods for extracting additional information from the returned echoes for tissue characterization. The ultimate goal is that this additional information be adequate for normal and pathological tissue differentiation, when the difference is not visually obvious in a conventional B-mode ultrasound image. This work focuses in the development of a tissue characterization method based on ultrasound data that is able to differentiate between healthy and various types of diseased soft tissue. We consider liver and breast tissues but the method may be modified to treat other types of tissue.

Ultrasonic interaction with tissue depends on the scattering structures which are involved. A three level model of the human liver scattering was first introduced by Bamber in 1979 (Bamber, 1979). He proposed a three component model which arises from superimposed structures with dimensions corresponding to cells, the liver parenchyma and larger structures such as blood vessels. Later, in 1986, a classification of scatterers based on their size or concentration relative to the resolution cell of the imaging system was introduced by Wagner and his team (Wagner et al., 1986; Insana et al., 1986). They classified the scatterers in two broad categories. The first class contains the so-called *diffuse scatterers*. They are related to the cells of soft tissue organs such as the liver and the breast. They are small in size (relatively to the resolution cell) and distributed randomly within the resolution cell. The interference of their echoes results in a fine grained texture in ultrasound images known as *speckle*. The process of interference was first described geometrically by Goodman (1975) for the laser speckle case, as a random walk of component phasors. The second class of scattering structures is related to the liver and breast parenchyma (liver and breast lobules and breast ducts) and blood vessels boundaries. These scatterers are large relatively to the resolution cell and thus can be resolved. They exist concurrently with the unresolved scatterers and are termed *coherent scatterers*. The presence of a coherent scatterer component leads to deviations from the Rayleigh scattering (Wagner et al., 1987; Insana et al., 1986; Tuthill et al., 1998). There is a major structural difference between the resolvable scatterers of the liver and breast. The liver lobules are organized in an almost periodic manner, resulting in a quasi-periodic coherent scattering component. The structure of the breast ducts and lobules is far from regular. Due to the quasi-periodic structure of the liver, the average spacing between the coherent scatterers has been extensively used to characterize the liver structure (Fellingham and Sommer, 1984; Landini and Verrazani, 1990). More recently, tissue characterization techniques exploit the information about the multicomponent scattering structure by modeling the RF signal with a two (Cohen et al., 1997; Varghese and Donohue, 1994) or three (Donohue et al., 1999; Abeyratne et al., 1996) component model and estimating quantities relevant to structural features. The two component models consider only echoes from periodic or quasi-periodic resolvable scatterers and diffuse (non-resolvable) scatterers, while the three-component models add a third type of echoes, produced by resolvable, non-periodic scatterers. The common characteristic of the works in (Varghese and Donohue, 1994; Donohue et al., 1999; Abeyratne et al., 1996) is that they do not decompose the signal into different components, but they use a multicomponent model to estimate specific features.

This paper presents a tissue characterization approach which includes a model, estimation algorithms and an evaluation technique. It is based on a decomposition of the RF echo of the liver and breast in accordance with the two major scattering

structures present in these tissues i.e., the quasi-periodic coherent scatterers related to the portal triads and lobules of the liver tissue and the ducts and lobules of the breasts tissue, and the diffuse scatterers related to the liver and breast tissue cells. Before embarking on the decomposition, a formal way of detecting whether or not an RF echo exhibits any specular scattering relative to the wavelength of the interrogating ultrasonic pulse is used. For the case of the liver, whose resolvable component is regular, minimum mean square (MMSE) estimates of the scattering space as well as the residual error variance of the diffuse component, that are efficient, computationally simple and result in accurate estimates in low signal-to-noise ratios (SNR) are derived. The MMSE estimates yield unique closed-form solutions and do not require a priori knowledge of the probability distribution function of the backscatter echo. For the case of the breast whose structure is far from regular, a decomposition based on thresholding the average power of the wavelet transform (WT) is developed. Both decomposition algorithms led to the estimation of parameters which are closely related to the tissue structure, such as the average spacing of the coherent scatterers of the liver and the energy of the coherent and diffuse scatterers. The estimated parameters are used for the characterization of the tissue through the use of empirical receiver operating characteristics (ROC) curves. The ROC analysis was chosen because it can quantify the diagnostic capacity of a system independently of the decision criterion. The proposed system is able to identify small lesions in the liver and breast (8 mm for the liver and 4 mm for the breast). This property, demonstrated with results, is very important because it implies that early cancer detection is possible.

This paper unifies and presents in one place work that has already been published (Cohen et al., 1997; Georgiou and Cohen, 2001; Georgiou et al., 2001), as well as new unpublished material such as ROC analysis results on breast tissue characterization based on 4 mm data records, liver tissue characterization results using the residual error variance of the diffuse component and ROC analysis on both the coherent scatterer spacings and residual error variance of the diffuse component of the liver. The rest of the paper is organized as follows. In Section 2, the RF echo model is introduced. The diffuse and coherent components are presented along with models describing their nature. The decomposition algorithms for both liver and breast are described in Section 3. Experimental results are presented in Section 4. We conclude the paper with a discussion in Section 5.

2. RF echo model

The RF echo signal is result of a three-dimensional convolution between the three-dimensional pressure wave and the three-dimensional tissue structure (Insana et al., 1990). However, under the assumptions of weak scattering, narrow ultrasound beam and linear propagation, the point scatterer model is an adequate model and has been widely used in the literature (Wagner et al., 1986; Varghese and Donohue, 1994; Donohue et al., 1999; Abeyratne et al., 1996; Wear et al., 1993). Let $h(t)$ be the ultrasound pulse shape and $s(t)$ be the scatterer distribution. Then the RF echo $y(t)$ is:

$$y(t) = s(t)h(t) = p(t) + d(t), \tag{1}$$

where $p(t)$ is the interaction of the pulse with the resolvable scatterers, i.e.,

$$p(t) = \sum_{n=1}^{N_c} p_n(t - \theta_n)h(t), \tag{2}$$

where N_c the number of coherent scatterers, θ_n are the time delays from the coherent scatterers to the receiver and p_n are their relative strengths. In Eq. (1), $d(t)$ is the interaction of the pulse with the randomly located diffuse scatterers given by:

$$d(t) = \sum_{n=1}^{N_s} d_n(t - \tau_n)h(t), \tag{3}$$

where N_s is the number of unresolvable scattering centers, τ_n are the time delays from the diffuse scatterers to the receiver, and d_n are their relative strengths. The RF echo $y(t)$ is sampled, resulting in an A-line $y(n)$.

As the RF signal results from a scatterer distribution which consists of mainly two components, the goal is to decompose it into these two

components. The mechanism that allows such a decomposition is the Wold-decomposition theorem (Picinbono, 1993),

$$y(n) = p(n) + d(n), \tag{4}$$

where:

(i) $d(n)$ is the non-predictable part;
(ii) $p(n)$ is completely predictable (the prediction error is 0);
(iii) $p(n)$ is uncorrelated with the prediction error of $d(n)$. This implies that $p(n)$ and $d(n)$ are orthogonal, i.e., $E\{p(n)d(s)\} = 0$ for all n and s.

The diffuse component $d(n)$ is modeled as a zero-mean autoregressive process of order p (AR(p)), driven by a zero mean white noise sequence $w(n)$ (not necessarily Gaussian) with variance σ^2, i.e.,

$$d(n) = \sum_{s=1}^{p} a_s d(n-s) + w(n). \tag{5}$$

The power spectral density (psd) $S(f)$ of $d(n)$ is given by (Picinbono, 1993)

$$S(f) = \frac{\sigma^2}{\gamma(f)} = \frac{\sigma^2}{\left|1 - \sum_{s=1}^{p} a_s \exp\{-\mathrm{j}2\pi f s\}\right|^2}. \tag{6}$$

Next we present the model for the coherent component of the liver and breast respectively.

2.1. Modeling the coherent component of the liver

For the case of liver, whose lobules are organized in a regular manner, the coherent component $p(n)$ is modeled as a periodic sequence with a period m, i.e., $p(n) = p(n+m)$, and hence $p(n)$ has a Fourier series representation

$$p(n) = \sum_{k=0}^{m-1} C_k \exp\left\{\frac{\mathrm{j}2\pi k n}{m}\right\}. \tag{7}$$

Given an N-point sequence ($N \geqslant m$) $p(n)$, $n = 0, 1, \ldots, N-1$, let $N_m = \alpha_m m$ be the largest integer smaller or equal to N which is divisible by m, and let $P_{N_m}(k)$ be its N_m-point DFT, i.e.,

$$P_{N_m}(l) = \sum_{n=0}^{N_m-1} p(n) \exp\left\{-\frac{\mathrm{j}2\pi n l}{N_m}\right\}, \tag{8}$$

where $l = 0, 1, \ldots, N_m - 1$. Let $k = 0, 1, \ldots, m-1$. Then $l = \alpha_m k + \beta$ with $\beta = 0, 1, \ldots, \alpha_m - 1$. After some calculations (Cohen et al., 1997) $P_{N_m}(\alpha_m k + \beta)$ reduces to:

$$P_{N_m}(\alpha_m k + \beta) = \begin{cases} N_m C_k, & \text{for } \beta = 0, \\ 0, & \text{for } \beta = 1, 2, \ldots, \alpha_m - 1. \end{cases} \tag{9}$$

In light of Eq. (9), the scattering spacing estimates will be derived directly based on the DFT data.

2.2. Modeling the coherent component of the breast

For the case of breast, where no regularity exists in the location of the resolvable scatterers, the coherent component $p(n)$ can be modeled by a superposition of Gaussian modulated sinusoids:

$$p(n) = \sum_{i=0}^{N_c} \frac{A_i}{\sigma_{ci}\sqrt{2\pi}} \exp\left\{\frac{(n-m_i)^2}{2\sigma_{ci}^2}\right\} \cos(\omega_c n), \tag{10}$$

where ω_c is the central frequency of the transducer, m_i indicates the location of the coherent scatterer, σ_{ci} is a parameter related to the transducer's bandwidth, A_i is related to the strength of the coherent scatterer and N_c is the number of coherent scatterers in the window examined. The only known parameter is ω_c.

3. Decomposition of tissues

In this section we explain first the decomposition for the liver and then the decomposition for the breast. A schematic diagram of the general approach is presented in Fig. 1.

3.1. Liver tissue decomposition

Let H_0 be the null hypothesis that stands for the absence of a resolvable coherent component, and H_1 the alternative hypothesis. Using the toroidal lattice approximation for the boundary conditions problem, the covariance matrix $[\Sigma]$ is circulant and diagonalizable by the Fourier matrix (Jain, 1989), i.e.,

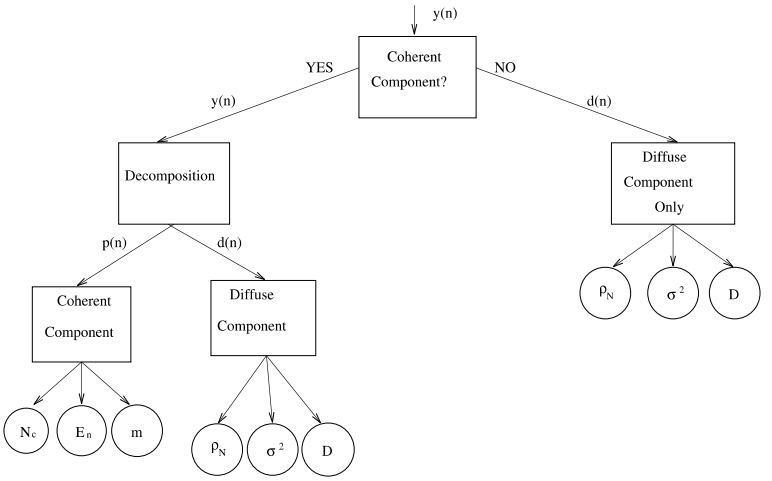

Fig. 1. Schematic diagram of the decomposition algorithm.

$$[F][\Sigma][F]^{t*} = [\Delta] \Rightarrow [\Sigma] = [F]^{t*}[\Delta][F]. \tag{11}$$

The Fourier transform is a unitary transform (Jain, 1989), hence, $\det[\Sigma] = \det[\Delta]$. It follows (Cohen et al., 1997) that

$$(\boldsymbol{y}-\boldsymbol{p})^t[\Sigma]^{-1}(\boldsymbol{y}-\boldsymbol{p}) = (\boldsymbol{Y}-\boldsymbol{P})^t[\Delta]^{-1}(\boldsymbol{Y}-\boldsymbol{P}) \tag{12}$$

where $\boldsymbol{y} = (y(0), y(1), \ldots, y(N_m-1))$, $\boldsymbol{p} = (p(0), p(1), \ldots, p(N_m-1))$, and $\boldsymbol{Y}$ and $\boldsymbol{P}$ be their respective N_m-point DFT, and $[\Delta]$ is the diagonal matrix $(1/N_m)\,\mathrm{diag}\,\{S(0), S(1/N_m), S(2/N_m), \ldots, S((N_m-1)/N_m)\}$, where S is given in Eq. (6). Let N_m be the largest number smaller or equal to N such that for any possible period m there exists a number in the closed set $[N_m, N]$ which is divisible by m. Under H_0, $\boldsymbol{P} = 0$ and hence $\boldsymbol{\Gamma}_0 = (\sigma_0^2, \boldsymbol{a}_0)$, and the likelihood function $p(\boldsymbol{y}|\boldsymbol{\Gamma}_0, H_0) = p(\boldsymbol{y}|\sigma_0^2, \boldsymbol{a}_0, H_0)$ is given by

$$p(\boldsymbol{y}|\boldsymbol{\Gamma}_0, H_0) = \prod_{k=0}^{N_{m-1}} \sqrt{\left(\frac{1}{2\pi N_m S_0(k)}\right)} \times \exp\left\{-\sum_{k=0}^{N_m-1} \frac{|Y(k)|^2}{2N_m S_0(k)}\right\}. \tag{13}$$

$S_0(k)$ is given in (6), with $f = (2\pi/N_m)k$. $\boldsymbol{a}_0$, σ_0^2 are the AR parameters and the residual error variance under H_0.

Under H_1 and for a given m, $\boldsymbol{\Gamma}_1 = \boldsymbol{\Gamma}_{1,m} = (\boldsymbol{C}_m, \sigma_{1,m}^2, \boldsymbol{a}_{1,m})$, and the likelihood function $p(\boldsymbol{y}|m, \boldsymbol{\Gamma}_{1,m}, H_1) = p(\boldsymbol{y}|m, \boldsymbol{C}_m, \sigma_{1,m}^2, \boldsymbol{a}_{1,m}, H_1)$ is given by

$$p(\boldsymbol{y}|m, \boldsymbol{\Gamma}_{1,m}, H_1) = \prod_{k=0}^{N_m-1} \sqrt{\left(\frac{1}{2\pi N_m S_{1,m}(k)}\right)} \times \exp\left\{-\sum_{k=0}^{N_m-1} \frac{|Y(k)-P_m(k)|^2}{2N_m S_{1,m}(k)}\right\}. \tag{14}$$

$S_1(k)$, $\boldsymbol{a}_{1,m}$ and $\sigma_{1,m}^2$ are defined similarly to $S_0(k)$, $\boldsymbol{a}_0$ and σ_0^2.

Before we embark on the process of estimating the unknown parameters, it is desirable to come up with a formal statistical decision rule to check whether or not there is enough evidence in the RF data to suggest the presence of a resolvable coherent component.

Let $p(H_0|\boldsymbol{y})$ and $p(H_1|\boldsymbol{y})$ be the a posteriori probability densities of H_0 and H_1, respectively, given the data $\boldsymbol{y}$. Let $p(H_0) = p(H_1)$. Then the minimum average probability of error decision rule is the Bayesian decision rule

$$\text{Accept } H_0 \text{ if } p(H_0|\boldsymbol{y}) > p(H_1|\boldsymbol{y}), \quad \text{otherwise accept } H_1. \tag{15}$$

This decision rule reduces to

$$\text{Accept } H_0 \text{ if } p(\boldsymbol{y}|H_0) > \max_m \{p(\boldsymbol{y}|H_{1,m})\}, \quad \text{otherwise accept } H_{1,m}, \tag{16}$$

where $H_{1,m}$ is the hypothesis of an assumed period of m. Note that this decision rule is unbiased (Cohen et al., 1997). A closed form expression for $p(\boldsymbol{y}|H_0)$ and $p(\boldsymbol{y}|H_{1,m})$ is given in (Cohen et al., 1997). In the absence of knowledge of the pdf, the unbiased decision rule in Eq. (16) is replaced by the decision rule

$$\text{Decide } H_0 \text{ if } d(0) > \max_m d_m(1), \quad \text{otherwise } H_{1,m}, \tag{17}$$

where

$$d(0) = -\frac{N_m}{2}\log\{\sigma_0^{2*}(m)\} - n(0)\log\left\{\frac{N_m}{2\pi}\right\}, \tag{18}$$

$$d_m(1) = -\frac{N_m}{2}\log\{\sigma_1^{2*}(m)\} - n(1)\log\left\{\frac{N_m}{2\pi}\right\}. \tag{19}$$

The first term in Eqs. (18) and (19) is the residual error and it is biased towards higher values of m. To compensate on the number of degrees of freedom, we introduce a penalty function (the second term of Eqs. (18) and (19)).

There are two possibilities for the distribution of the diffuse component irrespectively of the presence or absence of a coherent component, namely the Rayleigh and the non-Rayleigh case. For a more elaborate discussion on this subject please refer to our earlier work (Georgiou and Cohen, 1998). In the Rayleigh scattering case where the diffused component is Gaussian (Wagner et al., 1983), maximum likelihood (MLE) estimates for the Fourier series and the AR parameters under an assumed period m can be readily obtained by maximizing the joint likelihood of the data $\boldsymbol{y} = (y(0), y(1), \ldots, y(N_m - 1))$ $p(\boldsymbol{y}|\boldsymbol{C}_{1,m}, \boldsymbol{a}_{1,m}, \sigma_1^2(m), m)$ with respect to the unknown parameters $\boldsymbol{C}_{1,m} = (C_{0m}, C_{1m}, \ldots, C_{(m-1)m})$, $\sigma_1^2(m)$ and $\boldsymbol{a}_{1,m} = (a_{1m}, a_{2m}, \ldots, a_{pm})$. The MLE are efficient, and for relatively long records are unbiased. They result in accurate estimates in low SNR situations. Unfortunately, they require non-linear minimization. In the non-Rayleigh scattering case (Wagner et al., 1983) where the pdf of the data is unknown, MMSE estimates of the unknown parameters are computed. The MMSE estimates are computational simple, yield unique closed-form solutions, and do not require a priori knowledge of the probability distribution function of the backscatter echo. The MMSE estimates are computed as follows:

$$\sigma^2(m) = \frac{1}{(\alpha_m - 1)m}\left[\sum_{k=0}^{m-1}|Y(\alpha_m k) - N_m C_{km}|^2\gamma(\alpha_m k) + \sum_{\beta=1}^{a_m-1}\sum_{k=0}^{m-1}|Y(\alpha_m k + \beta)|^2\gamma(\alpha_m k + \beta)\right], \tag{20}$$

where

$$\gamma(\alpha_m k + \beta) = \left|1 - \sum_{s=1}^{p} a_{sm}\exp\left\{\frac{\mathrm{j}2\pi(\alpha_m k + \beta)s}{N_m}\right\}\right|^2 \tag{21}$$

and

$$C_{km}^* = \frac{Y(\alpha_m k)}{N_m}. \tag{22}$$

In general there is no guaranty that the estimation of $a_1, a_2, \ldots, a_p$ results into a positive definite spectrum. One possibility to overcome this problem is to use the fast Burg's algorithm for estimation the AR parameters, which is the only method that guarantees the AR process to be minimum phase, i.e., positive definite spectrum (Kay, 1988).

The physical parameters which are estimated through the decomposition and are used as tissue signatures are the following:

(1) Average liver spacing of the coherent component m which changes because the periodic structure of the liver lobules is destroyed when cancer is developed.
(2) The residual error variance of the diffuse component σ^2 which is related to the energy of the diffuse component.

3.2. Breast tissue decomposition

The assumption of regularly spaced coherent scatterers which allowed us to use the simplified model of Eq. (7), is not valid for the case of the breast. The existence of non-regularly spaced resolvable scatterers results in a non-stationary RF

echo. In this case, a time frequency analysis is more suitable (Loughlin, 1996; Tacer and Loughlin, 1998), We can choose between quadratic redundant time frequency representations (TFRs), for example the Wigner distribution, and liner redundant TFRs such as the short time Fourier transform, or the WT. The traditional quadratic TFRs are not suitable to multicomponent signals such as the ultrasound RF echo because they produce cross terms. Nevertheless, quadratic TFRs that suppress the cross terms are presented in (Choi and Williams, 1989; Jones and Baraniuk, 1995; Stankovic, 1996). The method in (Stankovic, 1996) is especially interesting, since it introduces quadratic TFRs that suppress the cross terms while preserving the auto terms. In this study we selected a linear TFR, namely the WT because of its flexibility and the good time and frequency localization (Bentley and McDonnell, 1994). It is chosen frequently for feature extraction in biomedical applications (Unser and Aldroubi, 1996). The WT has also been used for time or frequency decomposition in other fields. For example, Drumheller et al. (1995) used the WT successfully to identify and extract three acoustic components from the measured impulse response.

The underlying idea in the WT decomposition algorithm is to decompose the RF signal into the coherent and diffuse components in accordance with the point scatterer model for the RF data (Eq. (1)). The two components overlap in the time and frequency domain, therefore a time-frequency analysis is used to perform the decomposition. The selected TFR, i.e., the continuous WT is defined as the convolution of $y(n)$ with a scaled and dilated version of an admissible wavelet $\psi_0(n)$ (Torrence and Compo, 1998):

$$W(s,n) = \sum_{n'=0}^{N-1} y(n')\psi^*\left[\frac{(n'-n)}{sf_s}\right], \tag{23}$$

where ψ is the normalized wavelet.

Before embarking on the decomposition, the existence of a coherent component embedded in the RF signal is tested using the Kolmogorov Smirnov test for color field. More details about this test can be found in (Georgiou and Cohen, 1998), Section 4. If the test indicates absence of a coherent component, the diffuse component $d(n)$ is the RF echo $y(n)$ itself. Otherwise, the RF echo $y(n)$ is decomposed into its diffuse $d(n)$ and coherent $p(n)$ components using the wavelet decomposition described in (Georgiou and Cohen, 2001), Sections 3 and 4. The underlying idea of the extraction of the coherent component is simple. Fluctuations in the wavelet power over the range of scales are examined. Towards this end the scale-averaged wavelet power (SAP) is used, i.e.:

$$\overline{W}^2(n) = \frac{1}{J}\sum_{j=1}^{J} |W(s_j,n)|^2. \tag{24}$$

The SAP is used instead of the two-dimensional wavelet power because we are interested only in the time locations of the wavelet power concentrations.

The detection and time localization of the coherent scatterers is performed by thresholding the SAP with the following threshold:

$$\mu_w + \theta\sigma_w, \tag{25}$$

θ is a free parameter that needs to be tuned, μ_w be the mean of the SAP, i.e.,

$$\mu_w = \frac{1}{N}\sum_{n=0}^{N-1} \overline{W}^2(n) \tag{26}$$

and σ_w the standard deviation of the SAP around its mean value,

$$\sigma_w = \sqrt{\frac{1}{N-1}\sum_{n=0}^{N-1} \left(\overline{W}^2(n) - \mu_w\right)^2}. \tag{27}$$

Next the two components (or the one in the case of no coherent component) are used to estimate the features used in the tissue characterization. These features reflect the changes that occur in the tissue structure due to a disease, allowing us to discriminate between healthy and diseased tissue. The features of the coherent component are:

(1) the number of coherent scatterers per resolution cell N_c,
(2) the mean energy of the coherent scatterers E_n, which reflects differences in acoustic impedance between the large structures of breast (ducts and lobules i.e., parenchyma) and the surrounding tissue.

The features of the diffused component are:

(1) the residual error variance of the diffuse component σ^2,

$$\sigma^2 = \frac{1}{N}\sum_{k=0}^{N-1}\frac{\sigma^2}{|1-\sum_{s=1}^{p} a_s \exp\{j\frac{2\pi}{N}ks\}|^2}, \qquad (28)$$

(2) the Rayleigh scattering degree D, of the diffuse component $d(n)$, which describes the discrepancy between the empirical distribution $P(w)$ of the innovation process of $d(n)$ and the Gaussian distribution G,

$$D = \sup_{-\infty<w<\infty} |P(w) - G(w)|, \qquad (29)$$

(3) the normalized correlation coefficient of the diffuse component ρ_N, which reflects the correlations between neighboring diffuse scatterers in the tissue and depends on the density of the diffuse scatterers in the tissue,

$$\rho_N = \det\left[\frac{[\Delta]}{\sum_{k=0}^{N-1} NS(k)}\right] = \frac{\prod_{k=0}^{N-1} NS(k)}{\sum_{k=0}^{N-1} NS(k)}, \qquad (30)$$

where $[\Delta]$ is a diagonal matrix which diagonalizes the Fourier matrix $[F]$, i.e., $[F][\sigma][F]^{\dagger} = [\Delta]$, and its N diagonal elements $\{S(k) : k = 0, 1, \ldots, N-1\}$ are the sampled psd of d.

4. Results

There are two important aspects of testing the results of a tissue characterization method. The first aspect refers to a meaningful presentation of the results allowing easy interpretation. Towards this goal we selected the ROC analysis because it is the only method that can quantify the diagnostic capacity of a system independently of the decision criterion (Metz, 1989). Details about the empirical ROC computation that we use can be found in (Georgiou et al., 2001). The second aspect refers to the size of the tumors that a tissue characterization method can detect. In this study we present results that are based on windows of size 8 mm for the liver data 8 and 4 mm for the breast data.

4.1. Results on liver tissue characterization

In this section results on data from in vivo scans of liver tissue are presented. B-scan images of the liver were obtained in the Radiology Department of the Thomas Jefferson Hospital, Philadelphia, PA. The B-scans were obtained using an UltraMark-9 ultrasound system (ATL, Bothel, WA) using a transducer with a center frequency of 3.5 MHz, and a sampling frequency of 12 MHz. Clinical images from both patients and volunteers without any pathological report were examined. The data length along the depth axis was set to 128 samples, i.e., 8 mm of tissue approximately. The 8 mm window is short enough to ensure local wide sense stationarity of the signal, but also is long enough to ensure accurate estimation of the parameters. The window slid across the lateral direction by 1 A-line at a time and the estimates were recorded. The window also slid along the axial direction by 16 samples (i.e., 1 mm), and the estimates were recorded. The selection of the 1 mm depth that the window slides was arbitrary. The available database of liver B-scan images contained 84 images of 34 volunteers and patients. There were 44 liver B-scan images from 16 patients with cancer metastasis. Regions of interest (ROIs) on the tumor and away of the tumor were selected. The size of the ROIs was 1.25 cm in axial depth and 11 A-lines. The ROC curves for the average spacing and the residual error variance are shown in Fig. 2. The area under the ROC curve for the average spacing is $A_z = 0.748$. The residual error variance is the best parameter for liver tissue

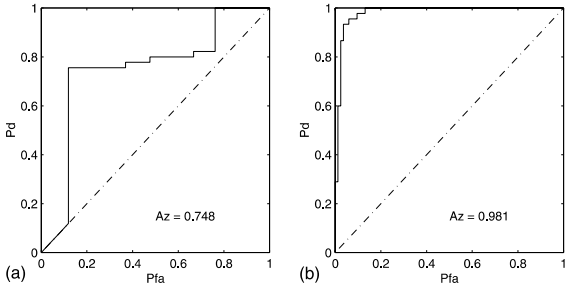

Fig. 2. ROC curves for normal vs cancerous liver tissue: (a) average scatter spacing m and (b) residual error variance σ^2.

classification. The ROC curve is presented in Fig. 2(b). The area under the ROC curve is $A_z = 0.981$. This parameter showed satisfactory diagnostic ability.

4.2. Results on breast tissue characterization

In this study we used 155 ultrasonic breast scans from 42 patients, obtained in the Radiology department of the Thomas Jefferson Hospital, Philadelphia, PA. A biopsy followed the ultrasound examinations and there is a detailed diagnosis for each patient. There are 37 carcinoma scans from 10 patients with in situ and infiltrating ductal carcinoma. There are 33 scans from 7 patients with fibrocystic changes and 3 patients with stromal fibrosis. There were 85 scans from 22 patients with fibroadenoma. The ultrasonic scans were obtained using a flat linear broadband array transducer with a nominal center frequency of 7.5 MHz on a clinical imaging system UltraMark-9, HDI, Advanced Technology Laboratories, Bothell, WA. The ATL system is a digital system. The frames were acquired just after beam forming. The sampling rate of the ATL system is 20 MHz. Two non-overlapping ROIs per scan, one on the lesion and another away from the lesion were selected by the authors. The size of the ROI's was 7.6–8 mm in axial depth and 10 lines in all cases. The axial size of the ROIs was chosen according to the size of smallest lesion of the database. The ROIs were not collected at the same depth because the tumors were not located at the same depth. Nevertheless, when possible, both ROIs corresponding to the same scan were collected on the same depth. Small variability was kept in the window size to eliminate variabilities of the estimated features due to the window size. The results for the 8 mm windows are presented in Tables 1 and 2. To save space, we present the area under the ROC curve (A_z) and not the ROC curve itself.

The residual error variance is the best parameter for classification. It works well for normal vs cancer for both the diffuse scattering and the diffuse and coherent scattering (all the corresponding ROCs (Tables 1 and 2) have area larger than 0.94). This parameter is also able to differentiate between malignant and benign tissue where benign tissue includes normal, fibrocystic and fibroadenoma tissue. The area under the ROC curve for the case of diffuse scattering is $A_z = 0.999$ and for the case of coherent and diffuse scattering $A_z = 0.893$.

Table 1
Area under the ROC curve (A_z) for the subclasses of images for which a coherent component was detected for the case of 8 mm windows

Categories	N_c	E_n	D	σ^2	$\log(\rho_N)$
Normal vs cancer	0.598	0.751	0.557	0.947	0.747
Normal vs fibroadenoma	0.558	0.862	0.744	0.945	0.863
Normal vs fibrocystic	0.688	0.669	0.521	0.947	0.875
Cancer vs fibroadenoma	0.558	0.866	0.706	0.501	0.718
Cancer vs fibrocystic	0.727	0.862	0.514	0.501	0.744
Benign vs malignant	0.576	0.763	0.542	0.893	0.758

Table 2
Area under the ROC curve (A_z) for the subclasses of images for which no coherent component was detected for the case of 8 mm windows

Categories	D	σ^2	$\log(\rho_N)$
Normal vs cancer	0.575	0.987	0.749
Normal vs fibroadenoma	0.538	0.936	0.868
Normal vs fibrocystic	0.574	0.947	0.912
Cancer vs fibroadenoma	0.554	0.955	0.724
Cancer vs fibrocystic	0.561	0.742	0.879
Benign vs malignant	0.568	0.999	0.887

We repeated the experiments for very short windows (4 mm). The results (in terms of A_z) are presented in Tables 3 and 4. We note that for the case of the 4 mm windows, no coherent part was found in all but one cancer case, so there was no ROC analysis for these cases (see the dashes in Tables 3 and 4).

The tissue characterization for the windows of 4 mm is performed using the diffuse component parameters, and more specifically the residual error variance σ^2. This feature gives $A_z = 0.987$ for differentiation between normal and cancerous tissue, and $A_z = 0.994$ for differentiation between benign and malignant tissue.

Table 3
Area under the ROC curve (A_z) for the subclasses of images for which a coherent component was detected for the case of 4 mm windows

Categories	N_c	E_n	D	σ^2	$\log(\rho_N)$
Normal vs cancer	–	–	–	–	–
Normal vs fibroadenoma	0.725	0.752	0.589	0.941	0.954
Normal vs fibrocystic	0.590	0.997	0.602	0.993	0.781
Cancer vs fibroadenoma	–	–	–	–	
Cancer vs fibrocystic	–	–	–	–	
Benign vs malignant	–	–	–	–	

Table 4
Area under the ROC curve (A_z) for the subclasses of images for which no coherent component was detected for the case of 4 mm windows

Categories	D	σ^2	$\log(\rho_N)$
Normal vs cancer	0.634	0.987	0.578
Normal vs fibroadenoma	0.608	0.979	0.501
Normal vs fibrocystic	0.603	0.991	0.790
Cancer vs fibroadenoma	0.511	0.803	0.663
Cancer vs fibrocystic	0.575	0.510	0.784
Benign vs malignant	0.620	0.994	0.500

5. Discussion

This paper considers the liver and breast tissue characterization problem. It presents a breast and liver tissue model, appropriate algorithms for parameters extraction and an evaluation method. The proposed method may be applicable to other types of tissue after appropriate development. The parameters extraction algorithms are based on a decomposition approach. The RF echo of the liver and breast is decomposed into a coherent and a diffuse component which are related to the resolvable and unresolvable scatterers of the tissue respectively.

Structural differences between the liver and breast led us to develop two different decomposition algorithms. The first algorithm was developed for the liver RF echo and was based on the quasi-periodic structure of the liver lobules. The decomposition allowed us to estimate several structural parameters, such as the mean scatterer spacing of the coherent component, the normalized correlation and the residual error variance of the diffused scatterers. The algorithm was applied to a large database of liver scans. Empirical ROC analysis was performed to evaluate the diagnostic abilities of the proposed system. The residual error variance and the average spacing of the coherent components showed good discrimination between normal and diseased tissue. The periodicity assumption for the coherent component can not be used for the breast because its structure is far from regular. To relieve this assumption we used a more general model for the coherent scatterers RF echo. The WT was the tool that allowed us to proceed with the decomposition and estimate the unknown parameters. The decomposition was based on thresholding the SAP of the WT. The proposed system estimates concurrently parameters related to the number and energy of the resolvable scatterers, the correlations between neighboring unresolvable scatterers and the density of the unresolved scatterers. These parameters are used as features for cancer detection and for differentiating between benign and malignant cases. The algorithm was tested on a large database of breast scans. The conclusion of our study indicates that the classification between normal and diseased tissue can be done reliably using the residual error variance of the diffuse component. The proposed algorithm is also capable of discriminating between benign and malignant pathologies of the breast tissue. This is a great advantage because most of the proposed tissue characterization methods have difficulties in discriminating malignant from benign tissue. This study also showed that the proposed system is able to detect and differentiate breast tissue abnormalities for very small window sizes (4 mm). This is very important because it implies that early detection of lesions based on ultrasound is possible.

References

Abeyratne, U.R., Petropulu, A.P., Reid, J.M., 1996. On modeling the tissue response from ultrasonic B-scan images. IEEE Trans. on Med. Imaging 15 (4), 479–490.

Bamber, J.C., 1979. Theoretical modeling of the acoustic scattering structure of human liver. Acoust. Lett. 3, 114–119.

Bentley, P.M., McDonnell, J.T.E., 1994. Wavelet transforms: an introduction. Electron. Commun. Engng. J. 6, 175–186.

Choi, H., Williams, W.J., 1989. Improved time–frequency representation of multicomponent signals using exponential kernels. IEEE Trans. Acoust. Speech Signal Process. 37 (6), 862–871.

Cohen, F.S., Georgiou, G., Halpern, E., 1997. WOLD decomposition of the backscatter echo in ultrasound images of soft tissue organs. IEEE Trans. Ultrason., Ferroelect. Freq. Contr. 44, 460–472.

Donohue, K.D., Forsberg, F., Piccoli, C.W., Goldberg, B.B., 1999. Classification of breast masses with ultrasonic scattering structure templates. IEEE Trans. Ultrason., Ferroelect. Freq. Contr. 46 (2), 300–310.

Drumheller, D.M., Hughes, D.H., O'Connor, B.T., Gaumond, C.F., 1995. Identification and synthesis of acoustic scattering components via the wavelet transform. J. Acous. Soc. Am. 97 (6), 3649–3656.

Fellingham, L.L., Sommer, F.G., 1984. Ultrasonic characterization of tissue structure in vivo human liver and spleen. IEEE Trans. Sonics Ultrason. 13, 418–428.

Georgiou, G., Cohen, F.S., 1998. Statistical characterization of diffuse scattering in ultrasound images. IEEE Trans. Ultrason., Ferroelect. Freq. Contr. 45, 57–64.

Georgiou, G., Cohen, F.S., 2001. Tissue characterization using the continuous wavelet transfer, Part I: Decomposition method. IEEE Trans. Ultrason., Ferroelect. Freq. Contr. 48 (2), 355–363.

Georgiou, G., Cohen, F.S., Piccoli, C.W., Forsberg, F., Goldberg, B.B., 2001. Tissue characterization using the continuous wavelet transfer, Part II: Application on breast RF data. IEEE Trans. Ultrason., Ferroelect. Freq. Contr. 48 (2), 363–373.

Goodman, J.W., 1975. Statistical properties of laser speckle patterns. In: Dainty, J.C. (Ed.), Laser Speckle and Related Phenomena. Springer-Verlag, New York, pp. 9–75.

Insana, M.F., Wagner, R.F., Brown, D.G., Hall, T.J., 1990. Describing small-scale structure in random media using pulse-echo ultrasound. J. Acoust. Soc. Am. 87, 179–192.

Insana, M.F., Wagner, R.F., Garra, B.S., Brown, D.G., Shawker, T.H., 1986. Analysis of ultrasound image texture via generalized Rician statistics. Opt. Engng. 25 (6), 743–748.

Jain, A.K., 1989. Fundamentals of Digital Image Processing. Prentice Hall, Englewood Cliffs, NJ.

Jones, D.L., Baraniuk, R.G., 1995. An adaptive optimal-kernel time–frequency representation. IEEE Trans. Signal Process. 43 (10), 2361–2371.

Kay, S.M., 1988. Modern Spectral Estimation. PTR Prentice Hall, Englewood Cliffs.

Landini, L., Verrazani, L., 1990. Spectral characterization of tissue microstructure by ultrasounds: a stochastic approach. IEEE Trans. Ultrason., Ferroelect. Freq. Contr. 37, 448–456.

Loughlin, P. (Ed.), 1996. Special issue on Time-Frequency Analysis: Biomedical Acoustical and Industrial Applications Proc. IEEE 84, 1195–1196.

Metz, C.E., 1989. Some practical issues of experimental design and data analysis in radiological ROC studies. Invest. Radiol. 9, 234–245.

Picinbono, B., 1993. Random Signals and Systems. Prentice Hall, Englewood Cliffs, NJ.

Stankovic, L.J., 1996. Auto-term representation by the reduced interference distributions: A procedure for kernel design. IEEE Trans. Signal Process. 44 (6), 1557–1563.

Tacer, B., Loughlin, P.J., 1998. Non-stationary signal classification using the joint moments of time-frequency distributions. Pattern Recognit. 31, 1635–1641.

Torrence, C., Compo, G.P., 1998. A practical guide to wavelet analysis. Bull. Am. Meteorol. Soc. 79, 61–78.

Tuthill, T.A., Sperry, R.H., Parker, K.J., 1998. Deviations from Rayleigh statistics in ultrasound speckle. Ultrason. Imaging 10, 81–89.

Unser, M., Aldroubi, A., 1996. A review of wavelets in biomedical applications. Proc. IEEE 84, 626–638.

Varghese, R., Donohue, K.D., 1994. Mean-scatterer spacing estimates with spectral correlation. J. Acoust. Soc. Am. 96, 3504–3515.

Wagner, R.F., Insana, M.F., Brown, D.G., 1986. Unified approach to the detection and classification of speckle texture in diagnostic ultrasound. Opt. Engng. 25, 738–742.

Wagner, R.F., Insana, M.F., Brown, D.G., 1987. Statistical properties of radio-frequency and envelope-detected signal with applications to medical ultrasound. Opt. Soc. Am. 4 (5), 910–922.

Wagner, R.F., Smith, S.W., Sandrik, J.M., Lopez, H., 1983. Statistics of speckle in ultrasound B-scans. IEEE Trans. Sonics and Ultrason. 30, 156–163.

Wear, K.A., Wagner, R.F., Insana, M.F., Hall, T.J., 1993. Application of autoregressive spectral analysis to cepstral estimation of mean scatterer spacing. IEEE Trans. Ultrason., Ferroelect. Freq. Contr. 40, 50–59.